(1) MARCH 1981

Dr. 2449
PPPL-1752
UC-20g

EFFECT OF NOISE ON THE STANDARD MAPPING

BY

C. F. F. KARNEY, A. B. RECHESTER,
AND R. B. WHITE

PLASMA PHYSICS LABORATORY

PRINCETON UNIVERSITY
PRINCETON, NEW JERSEY

This work supported by the U. S. Department of Energy Contract No. DE-AC02-76-CHO-3073. Reproduction, translation, publication, use and disposal, in whole or in part, by or for the United States Government is permitted.

PPPL–1752

EFFECT OF NOISE ON THE STANDARD MAPPING

Charles F. F. KARNEY

Plasma Physics Laboratory, Princeton University,

Princeton, New Jersey 08544, USA

Alexander B. RECHESTER

Plasma Fusion Center, Massachusetts Institute of Technology,

Cambridge, Massachusetts 02139, USA

Roscoe B. WHITE

Plasma Physics Laboratory, Princeton University,

Princeton, New Jersey 08544, USA

The effect of a small amount of noise on the standard mapping is considered. Whenever the standard mapping possesses accelerator modes (where the action increases approximately linearly with time), the diffusion coefficient contains a term proportional to the reciprocal of the variance of the noise term. At large values of the stochasticity parameter, the accelerator modes exhibit a universal behavior. As a result the dependence of the diffusion coefficient on stochasticity parameter also shows some universal behavior.

Key words: standard mapping; accelerator modes; area-preserving maps; diffusion; long-time correlations.

1. Introduction

The standard mapping,

$$v_t - v_{t-1} = -\epsilon \sin x_{t-1}, \qquad x_t - x_{t-1} = v_t, \tag{1}$$

is an important model with which to study the phenomenon of stochasticity [1]. Recently, Rechester and White [2] calculated the diffusion coefficient for this mapping with an added noise term δx_t in the equation for $x_t - x_{t-1}$. The random variable δx_t is sampled out of a normal distribution $f(\delta x_t; \sigma)$ of variance σ,

$$f(x;\sigma) = (2\pi\sigma)^{-1/2} \exp(-\tfrac{1}{2}x^2/\sigma).$$

The introduction of noise has profound effects on the long-time properties of (1). For instance, with $\sigma > 0$, the motion is ergodic; whereas, for $\sigma = 0$, the motion need not be ergodic even for large ϵ. ("Ergodic" here means that a time average for a single realization of the trajectory will be equal to a phase-space average where the phase space is defined by taking x and v modulo 2π.)

One consequence of the ergodicity of the motion when $\sigma > 0$ is that the diffusion coefficient may exhibit a $1/\sigma$ dependence for small σ. This happens whenever the mapping with $\sigma = 0$ has "accelerator modes" which are stable regions in which the particles are continually accelerated. We may easily see the origin of this $1/\sigma$ dependence. Ergodicity ensures that a fixed fraction of time is spent in each accelerator mode. As σ is decreased, the mode is visited less often while the duration of each visit is proportionately increased. (Only the noise can cause a particle to enter or leave an accelerator mode.) This leads to a diffusion consisting of a few large steps. Since the step size Δv and the duration of the step are both proportional to $1/\sigma$, the contribution to the diffusion coefficient also scales as $1/\sigma$. In this paper, we shall confirm the $1/\sigma$ dependence for two different types of noise. However, we expect similar behavior for any noise model.

The remainder of this paper is organized as follows: In section 2, the results of ref. 2 are interpreted in terms of the correlation function. This allows us to extend the result of ref. 2 to include other noise models and to determine the behavior of the diffusion coefficient when σ is small. In particular, we

predict the $1/\sigma$ dependence when there are accelerator modes present. Section 3 looks at the behavior of the diffusion coefficient numerically. The $1/\sigma$ dependence is confirmed and the dependence on ϵ is found. In section 4, we examine the ϵ dependence in more detail. We find that the accelerator modes, which give the $1/\sigma$ behavior, have a universal structure when ϵ is large. This means that the diffusion coefficient exhibits a dependence on ϵ which has some universal characteristics. The results are summarized in section 5.

2. The correlation function

We shall examine the standard mapping (1) with two different types of noise. With the first type, the standard mapping becomes

$$v_t - v_{t-1} = -\epsilon \sin x_{t-1} + \delta v_{t-1}, \qquad x_t - x_{t-1} = v_t + \delta x_t, \tag{2}$$

where δv_t and δx_t are random variables sampled from distributions $f(\delta v_t; \rho)$ and $f(\delta x_t; \sigma)$ respectively. This is a simple generalization of the system treated in ref. 2 so that the noise causes diffusion in both the v and x directions.

The effect of the second type of noise is described by

$$v_t - v_{t-1} = -\epsilon \sin x_{t-1}, \quad z_t - z_{t-1} = \delta z_t, \quad x_t - x_{t-1} = v_t - z_t + \delta x_t. \tag{3}$$

Here $(\delta x_t, \delta z_t)$ is a random point chosen with a distribution $g(\delta x_t, \delta z_t; \sigma)$ where

$$g(x, z; \sigma) = \exp(-\sigma)\,\delta(x, z) + [1 - \exp(-\sigma)]/(2\pi)^2\, u(x, z),$$

$\delta(x, z)$ is the Dirac delta function, and $u(x, z)$ is a uniform function equal to 1 if $|x| < \pi$ and $|z| < \pi$ and 0 otherwise. This noise term models the effect of large-angle scatterings. The effect of z in (3) is to provide an origin shift to v in the equation for $x_t - x_{t-1}$. The solution to (3) behaves as that of the noiseless standard mapping (1) as long as $(\delta x_t, \delta z_t)$ is $(0, 0)$. After an average of $1/\sigma$ (for small σ) iterations, a large-angle collision takes place which completely randomizes the particle's position in x and z.

Equations (2) and (3) represent examples of two distinct types of noise. In (2) the noise is diffusive; this is the limit in which the particle suffers frequent but small uncorrelated kicks. On the other hand, in the large-angle scattering model (3), the particle is rarely kicked by the noise but the kicks are large.

In the absence of noise, there exist small regular regions from which an orbit is excluded (assuming it started outside such a region). Noise destroys these regular regions allowing a particle to wander anywhere in phase space. In addition, the types of noise we consider in (2) and (3) maintain the area-preserving nature of the standard mapping because at any given time step they merely translate the phase space by some fixed amount. From this it follows that the motion is ergodic, i.e., that time averages can be replaced by phase-space averages.

The velocity-space diffusion coefficient is defined by

$$D = \lim_{t\to\infty} \frac{\langle (v_t - v_0)^2 \rangle}{2t}, \tag{4}$$

where the angle brackets denote an average over some appropriately chosen ensemble. An equivalent definition is [3]

$$D = \frac{1}{2}C_0 + \sum_{\tau=1}^{\infty} C_\tau, \tag{5}$$

where

$$C_\tau = \langle a_{t+\tau} a_t \rangle,$$

$a_t = v_{t+1} - v_t$ is the acceleration, and the average now includes an average over t. Because the motion is ergodic, we can replace the time average by a phase-space average coupled with an average over all realizations of the noise terms. (In calculating phase-space averages we use the periodicity of the mappings in the x and v directions so that the averaging need only be done over a $2\pi \times 2\pi$ square. However, when defining D and a_t, the periodicity in v is not used.) The result for C_τ will be independent of the ensemble chosen so the ensemble average can be ignored. Thus we have

$$C_\tau = \left\langle \int_0^{2\pi} \frac{dx_0}{2\pi} \int_0^{2\pi} \frac{dv_0}{2\pi} a_\tau a_0 \right\rangle, \tag{6}$$

where here the angle brackets mean an average over the distributions of all the noise terms appearing in $a_\tau a_0$. For instance, for the noise term in (2) we have

$$\langle\rangle = \int_{-\infty}^{\infty} f(\delta x_{\tau+1};\sigma)\,d\delta x_{\tau+1} \int_{-\infty}^{\infty} f(\delta v_\tau;\rho)\,d\delta v_\tau \cdots$$
$$\cdots \int_{-\infty}^{\infty} f(\delta x_1;\sigma)\,d\delta x_1 \int_{\infty}^{\infty} f(\delta v_0;\rho)\,d\delta v_0.$$

This operation is an identity in the limit $\sigma \to 0$ and $\rho \to 0$.

The first few C_τ are then found for (2) to be

$$C_0 = \tfrac{1}{2}\epsilon^2 + \rho, \qquad C_1 = 0,$$
$$C_2 = -\tfrac{1}{2}\epsilon^2 J_2(\epsilon)\exp(-\sigma - \tfrac{1}{2}\rho),$$
$$C_3 = -\tfrac{1}{2}\epsilon^2 J_1^2(\epsilon)\exp(-\sigma - \rho) + \tfrac{1}{2}\epsilon^2 J_3^2(\epsilon)\exp(-3\sigma - \rho).$$

Assuming that the sum in (5) can be truncated at $\tau = 3$, we have

$$D \approx \tfrac{1}{2}\rho + \tfrac{1}{2}\epsilon^2[\tfrac{1}{2} - J_2(\epsilon)\exp(-\sigma - \tfrac{1}{2}\rho) - J_1^2(\epsilon)\exp(-\sigma - \rho) + J_3^2(\epsilon)\exp(-3\sigma - \rho)].$$

With $\rho \to 0$ this agrees with the result obtained by Rechester and White [2]. We might expect the truncation to be accurate when ϵ greatly exceeds the stochasticity threshold, i.e., $\epsilon \gg 1$. This question will be examined in more detail below. This approach shows that the oscillations in D seen by Chirikov [1] are due to short-term correlations in the standard mapping and, contrary to his assertion, are not directly caused by the presence of accelerator modes.

The same calculation may be made for (3). Here we obtain

$$C_0 = \tfrac{1}{2}\epsilon^2, \qquad C_1 = 0,$$
$$C_2 = -\tfrac{1}{2}\epsilon^2 J_2(\epsilon)\exp(-2\sigma),$$
$$C_3 = [-\tfrac{1}{2}\epsilon^2 J_1^2(\epsilon) + \tfrac{1}{2}\epsilon^2 J_3^2(\epsilon)]\exp(-3\sigma),$$
$$C_\tau = \exp(-\sigma\tau)C_\tau(\sigma \to 0).$$

This result for C_τ comes about because the probability that at least one large-angle scattering takes place between a_0 and a_τ is $1 - \exp(-\sigma\tau)$. If no scattering takes place then the mapping is the same as the noiseless one.

In order to illustrate this method of computing the diffusion coefficient for another mapping, we consider the mapping obtained for the motion of an ion in a lower hybrid wave [3]. The mapping is

$$u_t - u_{t-1} = 2\pi\delta - 2\pi A \cos v_{t-1}, \qquad v_t - v_{t-1} = 2\pi\delta + 2\pi A \cos u_t$$

and we are interested in diffusion in the ρ direction where $\rho = \frac{1}{2}(v - u)$. We take A to be much larger than the stochasticity threshold $A \gg \frac{1}{4}$. Then the motion is approximately ergodic (even though there is no noise in this model). Furthermore, we expect (subject to the restrictions to be explored later in this section) that only a few terms in (5) contribute to D. So we have

$$D \approx \pi^2 A^2 [\tfrac{1}{2} + J_0(2\pi A)\cos(2\pi\delta) - J_1^2(2\pi A)\sin^2(2\pi\delta)],$$

where the first term in the brackets is the contribution from C_0 and the other terms come from C_1. Antonsen and Ott [4] have also derived this result using the method of paths in Fourier space [5].

The question of the accuracy of discarding the terms for $\tau > 3$ in (5) may most easily be addressed with the noise model employed in (3) because we need only determine the behavior of $C_{\tau>3}(\sigma \to 0)$. When $\sigma = 0$ and $\epsilon \gtrsim 1$, phase space may be divided into two regions: a large connected stochastic region and those parts of phase space within islands. A particle starting in either region stays forever in that region. It is useful to write C_τ as the sum of C_τ^{st} and C_τ^{is} which are the contributions to the integrals in (6) due to the stochastic and island regions respectively.

We shall assume that C_τ^{st} decays exponentially with increasing τ. So far as we know, this has not been proved for the standard mapping. The numerical evidence is that C_τ^{st} decays quite rapidly for small τ and large ϵ. The decay for larger τ is difficult to measure accurately because the error in the measurements of C_τ^{st} may exceed the value of C_τ^{st}. (Grebogi et al. [6] have suggested that the decay may be slower than exponential for some ϵ.)

The contributions due to the island region may be evaluated quite accurately because, within a given island, the time-averaged acceleration is a constant α_i (i is a subscript labelling the various islands). The frequency of oscillation around an island is typically of order unity. Therefore C_τ^{is} consists of a mean part (independent of τ) equal to $Q = \sum_i \alpha_i^2 A_i / A_0$ plus a part which oscillates with a frequency of about unity. A_i is the area of the ith island and $A_0 = (2\pi)^2$ is the total area of phase space.

We are now in a position to assess the contributions to D of C_τ^{st} and C_τ^{is} when σ is finite. The sum

over C_τ^{sl} probably converges rapidly so that a truncation at some fairly low τ is quite accurate. Since, in that case, only the terms for small τ contribute to D, a small amount of noise has little effect on this contribution. The oscillatory part of C_τ^{sl} may similarly be neglected when evaluating D since its sum when weighted by $\exp(-\sigma\tau)$ is on the order of σ. The mean part of C_τ^{sl}, on the other hand, increases D by

$$\begin{aligned} D_{sl} &= \frac{1}{2}C_0^{sl} + \sum_{\tau=1}^{\infty} C_\tau^{sl} \approx Q\left(\frac{1}{2} + \sum_{\tau=1}^{\infty}\exp(-\sigma\tau)\right) \\ &= \frac{1}{2}Q\coth(\tfrac{1}{2}\sigma) \approx Q/\sigma \\ &= \sum_i \frac{a_i^2 A_i}{\sigma A_0}. \end{aligned} \tag{7}$$

This will be nonzero if at least one of the islands is an accelerator mode, i.e., $a_i \neq 0$ for some i. In these modes, a particle, instead of returning to the original island after N iterations, goes to the image of that island displaced upwards or downwards in y by some multiple of 2π. Such a mode is called an Nth-order accelerator mode. (In fact, due to the symmetries of the standard mapping, accelerator modes come in pairs with $A_{2i} = A_{2i-1}$ and $a_{2i} = -a_{2i-1}$.) So, if accelerator modes exist, σ can be chosen so that D_{sl} and hence D are arbitrarily large.

Accelerator modes are best found by looking for stable accelerating fixed points. Around each such fixed point there will be an accelerator mode. Several first- and second-order accelerating fixed points for (1) are cataloged in table I. Chirikov [1] gives

$$\epsilon_0 = 2\pi n < |\epsilon| < [(2\pi n)^2 + 16]^{1/2} = \epsilon_1 \tag{8}$$

with n being an integer as the condition for the stability of first-order fixed points. The magnitude of the acceleration of the accelerator mode associated with such fixed points is $2\pi n$. Actually the first-order modes exist beyond ϵ_1. The second-order fixed points which are marked by asterisks and which follow the first-order fixed points in the table are the result of the first-order fixed point becoming unstable and giving rise to 2 stable second-order fixed points. The accelerating regions around these second-order fixed points are best thought of as being a continuation of the first-order accelerator mode.

The physical explanation of the $1/\sigma$ divergence was given in section 1. Here we will cast that explanation into more quantitative terms. Consider a particle that has just been placed in an accelerator mode by a collision. When σ is small, the probability that it survives in that mode for longer than a time t is $P(t) = \exp(-\sigma t)$. (This is just the probability that there is no collision during the time t.) The probability that it leaves between times t and $t + dt$ is $p(t)dt$ where $p(t) = -dP(t)/dt = \sigma \exp(-\sigma t)$. From (4), the contribution to the diffusion coefficient from the accelerator modes is

$$D_{i\sigma} = \sum_i \frac{1}{2} \frac{\int_0^\infty a_i^2 t^2 p(t) dt}{\int_0^\infty t p(t) dt} \frac{A_i}{A_0} \tag{9}$$

The factor A_i/A_0 is the fraction of time a particle spends in the ith accelerator mode. Substituting for $p(t)$, we have $D_{i\sigma} = Q/\sigma$ which agrees with (7).

The same considerations apply to the standard mapping with noise given by (2). In this case, the form of $p(t)$ is not known; it will in fact depend on the size of the accelerator mode. However, we do expect the duration of a particle's stay in an accelerator mode to be approximately Δ^2/σ (for $p = 0$) where Δ is the scale length of the island. This is to be compared with an average duration of $1/\sigma$ for the large-angle scattering case (3). Since Δ is usually quite small, the coefficient of the $1/\sigma$ term in D for (2) should be smaller than that for (3). These considerations will be refined in section 4, when we will be able to make more accurate scaling arguments.

In the next section we numerically confirm the $1/\sigma$ dependence and explore the dependence of D on ϵ.

3. Numerical evaluation of the diffusion coefficient

In order to measure the diffusion coefficient numerically we adopted a method based on (5) which is designed to handle systems with long correlations. The trajectories of J particles with random initial conditions (with a uniform distribution) are advanced to $t = kT$ according to either (2) or (3). A

correlation function is defined for the kth iterate of the map for each trajectory by

$$C_\tau^k = \frac{1}{T-\tau}\sum_{t=0}^{T-\tau-1} a_t^k a_{t+\tau}^k$$

where $a_t^k = v_{t+1} - v_t$ is the acceleration due to k iterates of the map. A diffusion coefficient based on the jth trajectory is given by

$$D_j = \frac{1}{2k}C_0^k + \frac{1}{k}\sum_{\tau=1}^{L} C_\tau^k.$$

The final value of D is obtained by averaging D_j over j. The standard deviation of D_j divided by $\sqrt{J}$ is used to give a measure of the error in D.

In this method, correlations up to a time separation of kL are retained. With $T = 1$ and $L = 0$, we recover the "standard" method which is based on (4); in order to obtain accurate results in this case J must be large. Here we do not take J to be large; however, good statistics are obtained because we take $T - L \gg 1$ so that there are many observations of each C_τ^k. Normally we take J to be 64 which allows us to make full use of the vectorization capabilities of the Cray-1 computer on which the computations of D are performed.

In fig. 1, we show the σ dependence of D for (2) with $\rho = 0$ and $\epsilon = 6.6$ and 12.8. D is normalized to its quasi-linear value $D_{ql} = \frac{1}{4}\epsilon^2$. These values of ϵ were chosen to satisfy (8) for $n = 1$ and 2. We see that D does have a $1/\sigma$ dependence for small σ. The values of σ at which this dependence becomes evident are about 10^{-4} and 10^{-5} for $\epsilon = 6.6$ and 12.8. The values for D for $\sigma = 10^{-7}$ greatly exceed the numerical values given in ref. 2. Since orbits of length 50 were used in those computations, the effect of the accelerator modes was largely suppressed.

Also shown in fig. 1 is D for (3) with $\epsilon = 6.6$. As expected, the coefficient of the $1/\sigma$ term is nearly *100 times larger than for (2).*

Taking the limit $D(\sigma \to 0)$ gives an infinite result from the $1/\sigma$ term. If we interchange the limits so that we take $\sigma \to 0$ before $t \to \infty$ in (4), the value of D depends on how the initial conditions are chosen since the motion in this case is not ergodic. If an ensemble is defined by chosing initial

conditions uniformly in phase space, D is infinite because some trajectories will be accelerating. This is then consistent with the value of D obtained by taking the limit $\sigma \to 0$ after $t \to \infty$. A more "natural" ensemble is obtained if we restrict the initial conditions to the stochastic region of phase space. Figure 1 shows the value of the D for $\epsilon = 6.6$ and $\sigma = 0$ with such initial conditions. The error in this measurement of D is quite large even though long trajectories were used in the computation. This probably arises because the stochastic region includes a "sticky" portion close to the accelerator modes. A particle which wanders into this portion of phase space may still spend a long time accelerating even though the trajectory is still stochastic. The properties of these sticky regions around islands need more thorough study if the diffusion coefficient for $\sigma = 0$ is to be understood.

No enhancement of D was detected in the ranges of ϵ where second-order accelerator modes exist. Because these modes are much smaller than the first-order accelerator modes the value of σ at which they begin to contribute significantly is so small that prohibitively long runs would have to be made to detect any effect numerically.

Next we turn to the behavior of D as a function of ϵ. Here we hold σ fixed and equal to 3×10^{-6} and ϵ is varied in and somewhat beyond the ranges given by (8) with $n = 1$ and 2. The results are shown in fig. 2. D rises quite rapidly as soon as ϵ exceeds ϵ_0 for the first-order fixed point. At about one quarter and at about one half of the way through the interval (ϵ_0, ϵ_1), D is dramatically reduced. As we shall see this is due to the appearance of fourth- and third-order resonances. Nothing much happens to D at ϵ_1. Although the central fixed point becomes unstable at this value of ϵ, there is still a KAM surface of the original topology surrounding both the unstable first-order fixed point and the two new second-order stable fixed points. There is little change in the overall size of the island at this transition.

Perhaps the most noteworthy feature of fig. 2 is that the plots for both $n = 1$ and 2 are so similar. This suggests that there may be a universal structure for the accelerator modes. We pursue this subject further in the next section.

4. Universal behavior of accelerator modes

Referring to table I, we see that the accelerator modes exist only in a narrow range in ϵ. They are likewise present only in a small region of phase space. This effect becomes more pronounced as ϵ is increased and allows us to approximate the accelerator modes by a Taylor-series expansion of the mapping. We consider a general area-preserving map of the (x, y) plane which depends on a parameter k. We shift the origin and k so that the accelerator mode first appears at $(x, y) = 0$ and $k = 0$. We pick a frame traveling with the acceleration of the mode; therefore the constant terms which represent the acceleration are subtracted. We shall only directly treat accelerator modes which appear as a result of tangent bifurcations. Other higher-order fixed points which come from bifurcations of an existing accelerator mode will be treated as part of that accelerator mode. The linear terms of the mapping at $k = 0$ have the form

$$x_1 = (1 + a')x_0 + by_0, \qquad y_1 = b'x_0 + (1 - a')y_0,$$

with $a'^2 + bb' = 0$. Because the mode appears as a tangent bifurcation, the trace of the tangent mapping matrix is 2. By transforming (x, y) with

$$x = x' + a'y'/(a'^2 + b^2), \qquad y = -a'x'/b + by'/(a'^2 + b^2),$$

the linear mapping becomes

$$x'_1 = x'_0 + y'_0, \qquad y'_1 = y'_0.$$

A similar transformation is possible if $b = 0$ but $b' \neq 0$. The only case where the transformation is not possible is if $a' = b = b' = 0$ in which case the linear mapping is an identity. We now add the terms in the Taylor expansion which are quadratic in x and y and linear in k,

$$x'_1 = x'_0 + y'_0 + cx'^2_0 + dx'_0y'_0 + ey'^2_0 + fk \tag{10a}$$

$$y'_1 = y'_0 + c'x'^2_0 + d'x'_0y'_0 + e'y'^2_0 + f'k. \tag{10b}$$

We have taken $k \sim O(x^2)$. Unfortunately, this mapping is not in general area-preserving because the omitted cubic terms in the map also contribute to area preservation. However, we can make (10) conserve area by expressing four of the coefficients of the quadratic terms in terms of the other two.

The coefficients of $x_0'^2$, c and c', are taken as the independent ones. This choice is motivated by noting that the results are then independent of our choice of the direction of time. Thus when we invert (10), the coefficients of $x_1'^2$ depend only on c and c', whereas the other coefficients are linked in a more complicated way. Also, in some respects we may order y' as x'^2 [e.g., consider the positions of the fixed points of (10)]. The terms involving $x_0'y_0'$ and $y_0'^2$ are of the same order as the neglected terms. Therefore their coefficients should only be chosen to ensure the preservation of area; i.e.,

$$d' = 2(c' - c), \quad e' = (c' - c)^2/c', \quad d/d' = e/e' = c/c'.$$

Equation (10) may then be written as

$$x_1' = x_0' + y_0' + c[c'x' + (c' - c)y']^2/c'^2 + fk,$$

$$y_1' = y_0' + [c'x' + (c' - c)y']^2/c' + f'k.$$

Finally, we perform the transformations

$$x' = 2[x'' - (1 - c/c')y'']/c', \qquad y' = 2y''/c'$$

and

$$x'' = X, \qquad y'' = Y + 2K(f/f' - c/c'), \qquad k = -4K/(c'f')$$

to give

$$Y_1 - Y_0 = 2(X_0^2 - K), \qquad X_1 - X_0 = Y_1. \tag{11}$$

This is a universal mapping approximating the behavior of accelerating modes for large stochasticity parameter. All the transformations which give (11) are linear, and, with the exception of the last one which is just a shift of the origin, they are all independent of k (and K). For the first-order accelerator modes for the standard mapping (1) which appear at $\epsilon = 2\pi n$, the transformations reduce to

$$x = \pm\left(\frac{\pi}{2} + \frac{2}{\pi n}X\right), \quad v = \pm\left(-2\pi nt + \frac{2}{\pi n}Y\right), \quad \epsilon = 2\pi n + \frac{4}{\pi n}K. \tag{12}$$

The transformations leading to (11) are not well defined if the various coefficients satisfy unusual relationships. The first transformation is not possible if the linear term is an identity. If the motion around a stable Nth-order fixed point of a mapping is similar to rotation by an angle $2\pi p/q$ where p and q are integers, then the linear part of the qNth iterate of the map is an identity. But this does not

correspond to the first appearance of an accelerator mode. (It appeared with the Nth-order fixed point or sooner.) The transformations also fail if c' or f' is zero. In this case higher order terms have to be kept. This is what happens with the standard mapping at its (non-accelerating) fixed point which appears at $\epsilon = 0$ and $(x, v) = (0, 0)$. The same thing happens if we look at the second-order fixed points which appear when a first-order fixed point goes unstable (the fixed points marked with asterisks in table I). But here again such second-order fixed points are not the first occurrence of an accelerator mode in the neighborhood of parameter and phase space. They are treated by the second-order fixed points of (11) that appear for $K > 1$. Another form of degeneracy occurs if the exact mapping has, for instance, a real square root. Then quadratic terms in the mapping may be finite but still the cubic and quartic terms may not be neglected. An example of this is provided by the second iterate of (11).

Figure 3 illustrates this mapping for a particular value of K and also shows that it does indeed closely approximate the standard mapping near first- and second-order accelerator modes. Thus accelerator modes may be studied by examining (11) and how the transformations affect the diffusion.

We begin by cataloging some properties of (11). For $0 < K < 1$, (11) may be transformed into the Hénon quadratic map [7],

$$x_1 = x_0 \cos\alpha - (y_0 - x_0^2)\sin\alpha, \quad y_1 = x_0 \sin\alpha + (y_0 - x_0^2)\cos\alpha.$$

K is related to Hénon's parameter by $K = \sin^4(\alpha/2)$. The transformation between the two sets of coordinates is given by

$$X = \cos^2(\alpha/2)\sin(\alpha/2)w + Y/2 - \sin^2(\alpha/2), \quad Y = -2\cos(\alpha/2)\sin^2(\alpha/2)v,$$

and

$$w = x\cos(\alpha/2) + y\sin(\alpha/2), \quad v = -x\sin(\alpha/2) + y\cos(\alpha/2).$$

The transformation depends intimately on α (and hence on K) and becomes singular at $K = 0$ and 1.

For $K < 0$, (11) has no fixed points. It has two first-order fixed points for $K > 0$, $(X, Y) = (\mp\sqrt{K}, 0)$, which following ref. 7 we call I_1 and I_1' respectively. I_1' is always hyperbolic and so is unstable. I_1 is elliptic and therefore stable for $K < 1$. At $K = 1$, I_1 turns into a hyperbolic point with

reflection and two second-order fixed points are born. Thus the values $K = 0$ and $K = 1$ correspond to the parameter values ϵ_0 and ϵ_1 listed for the fixed points without asterisks in table I.

The second-order fixed points are stable for $1 < K < \frac{3}{4}$. This corresponds to the range in ϵ for which the fixed points labelled by asterisks in table I are stable. At $K = \frac{3}{4}$, a second bifurcation takes place giving rise to periodic trajectory of period 4. This trajectory in turn becomes unstable at $K = 1.2801$ when a period-8 cycle is born. The process of a period-2^m trajectory becoming unstable and producing a period-2^{m+1} trajectory continues. Greene et al. [8] show that it accumulates at $K = 1.2840 = \frac{1}{4}(1 + 1.2663)^2$. When K exceeds this value, they conjecture that (11) has no stable fixed points. Therefore, for large n the first-order accelerator modes exist for

$$\epsilon_0 = 2\pi n < \epsilon < \epsilon_2 \approx \epsilon_0 + 1.2840(\epsilon_1 - \epsilon_0) \approx 2\pi n + 1.2840 \times 4/(\pi n). \tag{13}$$

The map (11) has two main symmetry lines. They are the X-axis ($Y = 0$) which corresponds to the w axis in the Hénon map and the line $Y = K - X^2$. Reflection in one of the symmetry lines corresponds to reversing time. E.g., $Y = 0$ is the invariant line for the transformation $X = X' - Y'$, $Y = -Y'$ which turns (11) into its inverse.

In order to understand how (11) contributes to diffusion we must determine how large a region is trapped around the stable fixed points. We define an orbit to be trapped if X and Y remain bounded *for all time*. (Trapped orbits are the ones which contribute strongly to the diffusion because in the original mapping they are the ones that are perpetually accelerated.) Untrapped orbits escape to infinity with $Y \to +\infty$. It is straightforward to show that for $K \leq 2$ all particles with $Y \geq 10$ escape in this way. An approximate numerical test for being trapped is to check that $Y < 10$ during a large number of iterations. Figure 4 shows the extent of the trapped region along the two symmetry lines and its total area as functions of K. Figure 4b is just a rescaling of Hénon's fig. 2. The dips in the plots of the diffusion coefficient correspond to the large reductions in the size of the trapped region that occur for certain values of K. These are associated with the occurrence of higher-order resonances to the basic rotation about the I_1 [7]. Particularly large effects are produced by the fourth- and third-order

resonances. A stable period-four cycle exists for $\frac{1}{4} < K < 0.3044$. This is born at I_1 and in the process of moving away from this point destroys much of the stable region. A stable period-three cycle I_3 exists for $\frac{1}{2} < K < \frac{9}{16} = 0.5625$. Unlike other resonances this is born away from the associated lower-order fixed point I_1. I_3 moves further away from I_1 as K increases, while its unstable twin I_3' moves towards I_1. When I_3 goes unstable at $K = \frac{9}{16}$, I_3' is at I_1 causing the destruction of all stable regions in the neighborhood of I_1.

In order to make a more quantitative comparison between the behavior of the diffusion coefficient in fig. 2 and the behavior of (11), we must ascertain the effect of the transformations used to derive (11). We saw in section 2 that the contribution of an accelerator mode to the diffusion coefficient when the noise is due to large-angle scattering (3) is given by the area of the mode and its acceleration. Now the area of the accelerator mode is $4/(|b|c'^2)$ of the area of the trapped region of (11) (fig. 4c). So in the limit of small σ, the diffusion coefficient for (3) consists of a superposition over accelerator modes of forms of fig. 4c, linearly scaled by appropriate amounts in both directions. For a first-order accelerator mode, A_i the area of the mode scales as $1/n^2 \sim 1/\epsilon^2$ (12) while the acceleration varies as $a_i \sim n \sim \epsilon$. Thus from (7) we have $D_{is} \sim 1/\sigma$. The relative importance of the first-order modes with this noise model is given by $D_{is}/D_{qi} \sim 1/(\sigma\epsilon^2)$.

With the noise employed in (2), the situation is more complicated. The way diffusion due to σ and ρ enters (11) depends in a more involved way on the transformations used to derive (11). For instance, take the case where $\rho = 0$ (then all the diffusion due to the noise is in the x-direction). In (11) the diffusion is then along a line $Y = a'(a'^2 + b^2)X/b^2$. So the effect of each accelerator mode as a function of K depends on what this direction is. However, in (2) the important accelerator modes are the first-order ones and for these modes the transformation to (X, Y) takes the particularly simple form (12). The only way the transformation changes as n is changed is by an overall scale factor. The effect of the noise will then only depend on the ratio of ρ to σ (apart from a constant factor).

In order to find the effect of a first-order accelerator mode in (2) on the diffusion coefficient, we go back to the expression for D_{is} given in (9). Now $p(t)$ is no longer a probability since it is not

normalizable. It may be defined as follows. Imagine scattering infinitely many particles at the boundary of the trapped region. (The number of particles has to be infinite because almost all of them leave the trapped region immediately.) Suppose the number which are left after a time t is $P(t)$. The number which leave between t and $t + dt$ is then $p(t)dt$ where $p(t) = -dP(t)/dt$. Before applying (9), we must also ensure that σ and ρ are small so that each visit to the accelerator mode is uncorrelated with the previous one. (If σ or ρ is not small, the particle may be immediately scattered back into the trapped region after being scattered out of it, instead of being swept far away from the island. This effectively increases the area of the trapped region. Such considerations were not necessary for the large-angle scattering model.) Taking $\rho = 0$, we have $p(t) \sim q(\sigma t/\Delta^2)$ where q is some function which, for a given K, applies for all first-order accelerator modes and which is independent of σ. Δ is the scale length of the island which from (12) is proportional to $1/n$. Here again, σ must be small to be able to write $p(t)$ in this way because we need to be able to separate the slow time scale of the motion due to the noise in (2) from the fast time scale due to the standard mapping itself. This form for $p(t)$ applies for any diffusive noise model if we regard σ as a measure of the extent of the Green's function response after a unit of time under the action of the noise alone. Using (9), we find that, when ϵ satisfies (13), $D_{1s} \sim 1/(\pi\epsilon^2)$ and $D_{1s}/D_{ql} \sim 1/(\sigma\epsilon^4)$. This is confirmed by fig. 2, where we see that D/D_{ql} decreases by roughly a factor of 16 when ϵ is doubled.

5. Conclusions

When noise is added to the standard mapping the diffusion coefficient consists of two parts. One part is primarily due to short-term correlations in the stochastic region of phase space and this part exhibits nearly sinusoidal oscillations [2]. The other part is proportional to the inverse of the noise parameter σ and exists only when accelerator modes are present. When the noise is weak, this latter part dominates. The role of the noise is to ensure that every trajectory eventually visits the accelerator modes. This effect has been confirmed numerically for the first-order accelerator modes. These modes exist in windows given by (13) and their relative importance decays as ϵ^{-4} for diffusive noise (2) and

as ϵ^{-2} for large-angle scattering (3). Although many higher-order accelerator modes exist (see table I), they are so small that they do not contribute significantly to D for the values of σ that can be dealt with computationally. In the absence of noise the diffusion coefficient is not fully defined until the ensemble in (4) is specified. However, anomalies in the diffusion coefficient are seen even when the ensemble in (4) is taken to be trajectories in the stochastic region. This is apparently because trajectories can be greatly accelerated while in the vicinity of the accelerator modes.

We showed in section 4 that the accelerator modes exhibit a universal behavior. Depending on the noise model, the diffusion coefficient therefore exhibits some universal features as the parameter ϵ is varied.

Similar effects are expected in other mappings which allow accelerator modes. Such mappings are ones which are periodic in the velocity direction. For example, an anomalously large diffusion coefficient was found at a certain value of the parameter for the mapping studied in ref. 3. (The divergent behavior of the diffusion coefficient for this case has been noted by Antonsen and Ott [4].) However, such mappings are often derived as approximations to mappings which are not periodic in the velocity direction. For instance (1) may be derived from similar mappings in which ϵ is effectively a function of v, $\epsilon(v)$ [9]. These more general mappings do not have accelerator modes. Nevertheless, if the dependence of ϵ on v is weak, we still expect there to be some effect due to the presence of the "latent" accelerator modes. These are channels in phase space which allow particles to be uniformly accelerated from a velocity v_0 such that $\epsilon(v_0) \approx \epsilon_0$ to a velocity v_2 such that $\epsilon(v_2) \approx \epsilon_2$ (ϵ_0 and ϵ_2 being the parameter values for the birth and death of an accelerator mode in the standard mapping). No noise is required to bring particles into these channels. This short cut will result in an enhancement of the diffusion coefficient between v_0 and v_2. Diffusion on longer velocity-space scales will still be limited by the slower diffusion elsewhere.

Acknowledgments

This work was supported by the U.S. Department of Energy under Contracts DE–AC02–76–CH03073 and DE–AS02–78ET53074. This work was begun while two of us (C.F.F.K. and A.B.R.) were attending the Aspen Institute of Physics. We would like to thank H. A. Rose whose valuable comments stimulated us to look into this problem, and R. S. MacKay and P. J. Morrison for useful discussions.

References

[1] B. V. Chirikov, Phys. Rept. 52 (1979) 263.

[2] A. B. Rechester and R. B. White, Phys. Rev. Lett. 44 (1980) 1586.

[3] C. F. F. Karney, Phys. Fluids 22 (1979) 2188.

[4] T. M. Antonsen and E. Ott, Plasma Preprint PL-81-018, University of Maryland (1980).

[5] A. B. Rechester, M. N. Rosenbluth, and R. B. White, Plasma Physics Rept. PPPL-1678, Princeton University (1980).

[6] C. Grebogi, A. K. Kaufman, and H. D. I. Abarbanel, Bull. Am. Phys. Soc. 25 (1980) 988.

[7] M. Hénon, Quarterly of App. Math. 27 (1969) 291.

[8] J. M. Greene, R. S. MacKay, F. Vivaldi, and M. J. Feigenbaum, Plasma Physics Rept. PPPL-1745, Princeton University (1981).

[9] A. J. Lichtenberg, M. A. Lieberman, and R. H. Cohen, Physica 1D (1980) 291.

Tables

Table 1. First- and second-order stable accelerating fixed points for the standard mapping (1). Here, N is the order of the fixed point and α is its mean acceleration. The subscripts 0 and 1 denote the values of ϵ, x, and v when the fixed point first appears and when it becomes unstable. These fixed points together with those generated from these by the symmetries of (1) give all the first- and second-order accelerating fixed points for $|\epsilon| \leq 20$. The entries labelled with asterisks result when the preceding first-order point becomes unstable.

N	$\lvert\alpha\rvert/(2\pi)$	ϵ_0	$(x_0, v_0)/(2\pi)$	ϵ_1	$(x_1, v_1)/(2\pi)$	$\epsilon_1 - \epsilon_0$
2	1/2	4.0236	0.3957, 0.1951	4.0921	0.3846, 0.2159	0.0685
1	1	6.2832	0.2500, 0.0000	7.4484	0.1598, 0.0000	1.1652
*2	1	7.4484	0.1598, 0.0000	7.7134	0.2083, 0.0928	0.2650
2	1/2	8.6789	0.5416, 0.3214	8.6883	0.5402, 0.3272	0.0093
2	1	9.8226	0.4526, 0.2294	9.8288	0.4516, 0.2342	0.0062
2	1/2	9.9166	0.2087, 0.2627	9.9311	0.2177, 0.2741	0.0145
2	3/2	10.9101	0.3678, 0.1409	10.9175	0.3666, 0.1459	0.0074
1	2	12.5664	0.2500, 0.0000	13.1876	0.2010, 0.0000	0.6213
*2	2	13.1876	0.2010, 0.0000	13.3385	0.2260, 0.0494	0.1508
2	1/2	14.3918	0.5939, 0.3629	14.3949	0.5934, 0.3656	0.0031
2	3/2	15.0416	0.2254, 0.1826	15.0452	0.2288, 0.1866	0.0036
2	1	15.2394	0.5270, 0.2954	15.2413	0.5267, 0.2976	0.0019
2	3/2	15.9607	0.4700, 0.2378	15.9623	0.4698, 0.2398	0.0016
2	1	15.9966	0.2271, 0.2598	15.9992	0.2301, 0.2632	0.0027
2	2	16.6679	0.4142, 0.1810	16.6697	0.4139, 0.1831	0.0017
2	1/2	16.9287	0.2278, 0.3341	16.9321	0.2312, 0.3380	0.0034
2	5/2	17.4630	0.3515, 0.1168	17.4657	0.3510, 0.1193	0.0027
1	3	18.8496	0.2500, 0.0000	19.2693	0.2167, 0.0000	0.4197
*2	3	19.2693	0.2167, 0.0000	19.3728	0.2335, 0.0334	0.1035

Figure Captions

Fig. 1. The dependence of D/D_{ql} on σ where $D_{ql} = \frac{1}{4}\epsilon^2$. The bars indicate the error ($\pm$ one standard deviation). The lower two curves are for the diffusive noise model (2) with $\rho = 0$ and (a) $\epsilon = 6.6$ and (b) $\epsilon = 12.8$. The upper curve (c) is for the large-angle scattering model (3) and $\epsilon = 6.6$. The dashed lines show the $1/\sigma$ dependence. The point with the lowest value of σ on each curve was calculated with $kT = 2 \times 10^5$ and $kL = 10^3$. Lower values of these parameters were used for the larger values of σ. The point on the right (d) gives D/D_{ql} for $\sigma = 0$ and initial conditions in the stochastic region. Here $kT = 10^6$ and $kL = 5 \times 10^5$.

Fig. 2. D/D_{ql} as a function of ϵ for the standard mapping with diffusive noise (2) with $\rho = 0$ and $\sigma = 3 \times 10^{-6}$. The bars show the error as in fig. 1. Here $kT = 6 \times 10^6$ and $kL = 3 \times 10^4$.

Fig. 3. *Comparison of the quadratic mapping* (11) *with the standard mapping* (1) *in the regions of accelerator modes.* The first figure (a) shows trajectories for the mapping (11) with $K = 0.265$ with 9 different initial conditions. There is a first-order island at the origin whose center is I_1. The other two large islands are part of a chain of 4 fourth-order islands. The other figures (b and c) show trajectories for the mapping (1) with $\epsilon = 18.9620$ and 15.0425 where first- and second-order accelerator modes exist. The coordinates (x, v) in (1) have been transformed to (X, Y) according to the prescription given in Section 4 with $K = 0.265$, i.e., for (b) the transformation is (12) with $n = 3$; and for (c) it is $x/(2\pi) = 0.2254 - 10^{-3}(3.4298X + 0.0019Y + 0.0001K)$, $v/(2\pi) = 0.1826 - \frac{3}{2}t - 10^{-3}(3.9784X - 0.2721Y - 0.0119K)$, and $\epsilon = 15.0416 + 3.6453 \times 10^{-3}K$.

Fig. 4. The trapped region of phase space for the quadratic mapping (11). Plots (a) and (b) shows the intersection of the trapped region with the two symmetry lines $V = K - X^2$ and $V = 0$. The trapped region is represented in black. These plots are calculated with a resolution of 0.002 in X and K. Trajectories of length 10 000 were used in the test for being trapped. The curve (c) shows the total area A of the trapped region. This was calculated with a resolution of 0.005 in X and Y and at intervals of 0.01 in K. Here the trajectory length was 1000.

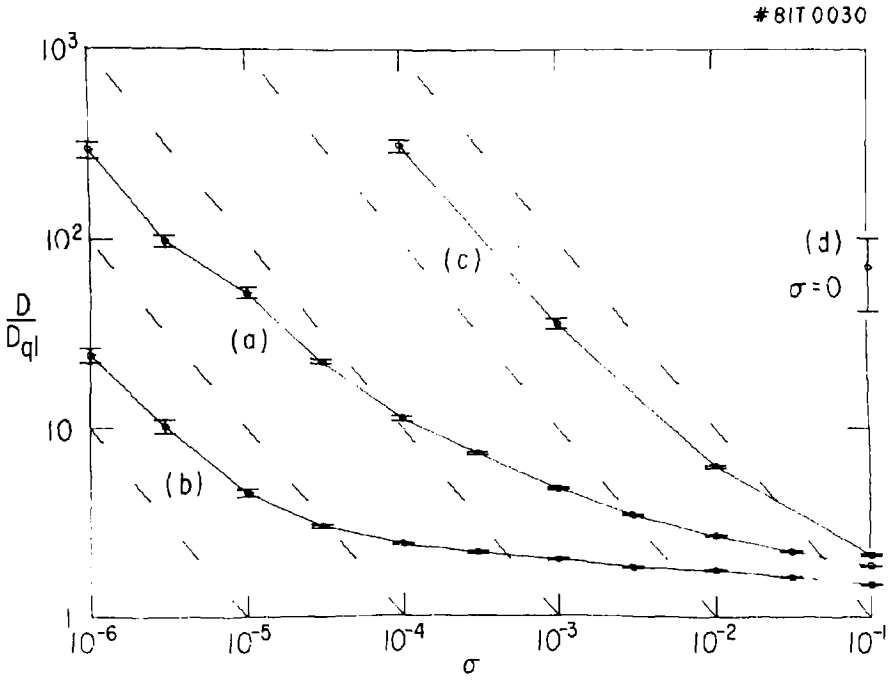
#81T0030
10^3
10^2
10
1
$\frac{D}{D_{ql}}$
(a)
(b)
(c)
(d)
$\sigma = 0$
10^{-6}
10^{-5}
10^{-4}
10^{-3}
10^{-2}
10^{-1}
σ

Figure 1

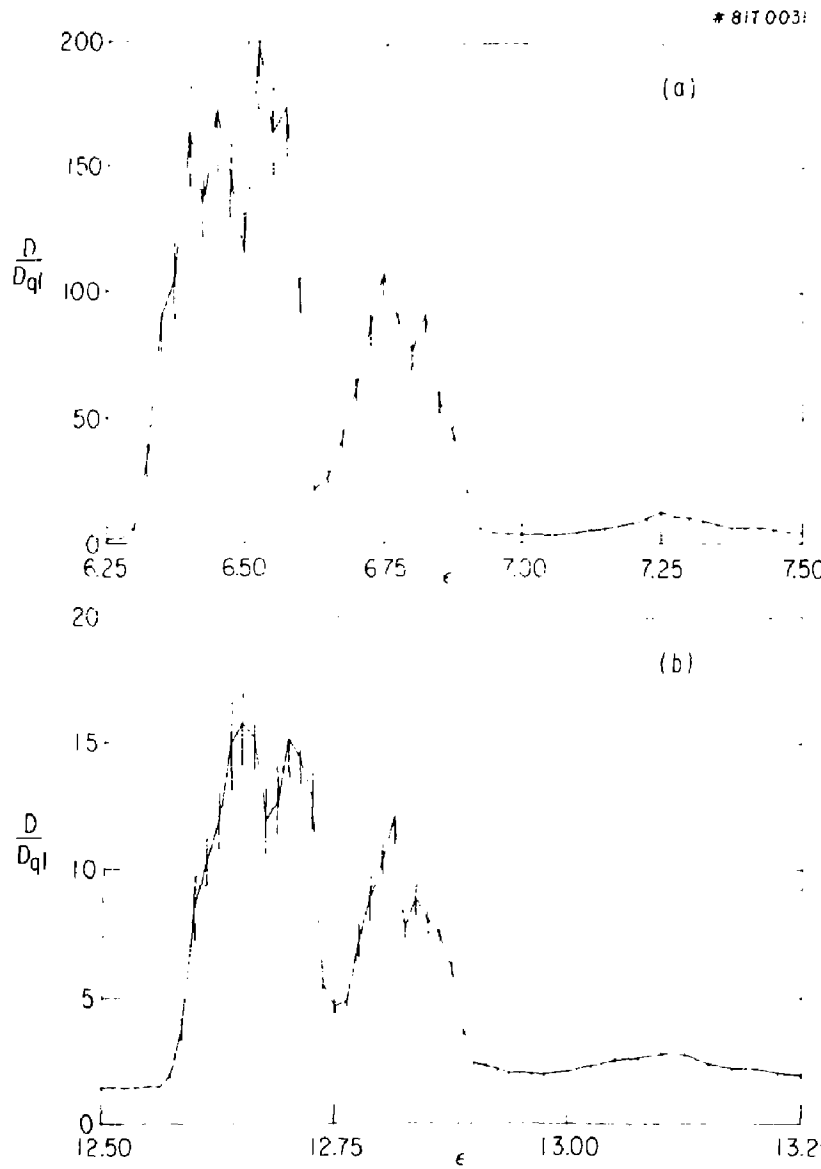
#817003
(a)
200
150
100
50
0
D/Dql
6.25
6.50
6.75
7.00
7.25
7.50
ε
(b)
20
15
10
5
0
D/Dql
12.50
12.75
13.00
13.25
ε

Figure 2

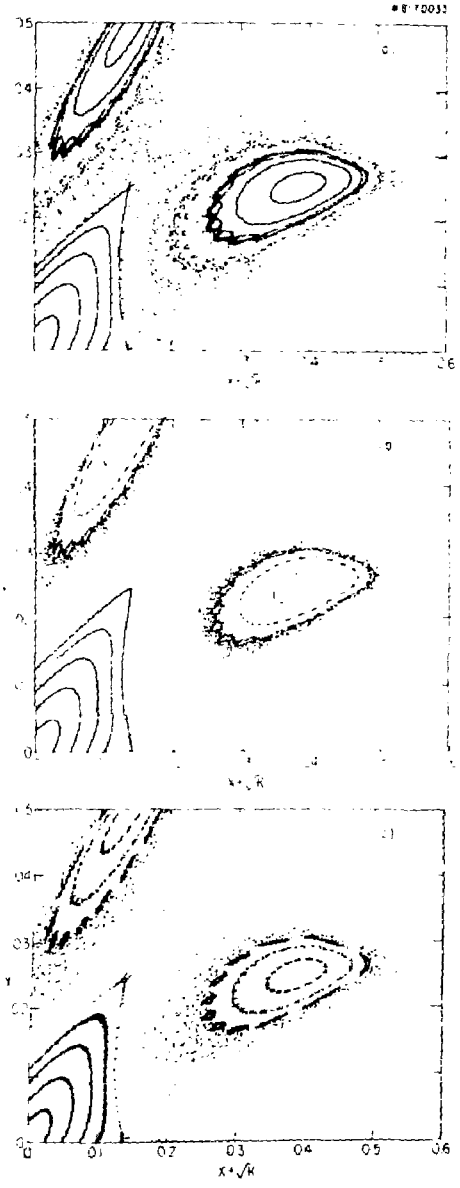

Figure 3

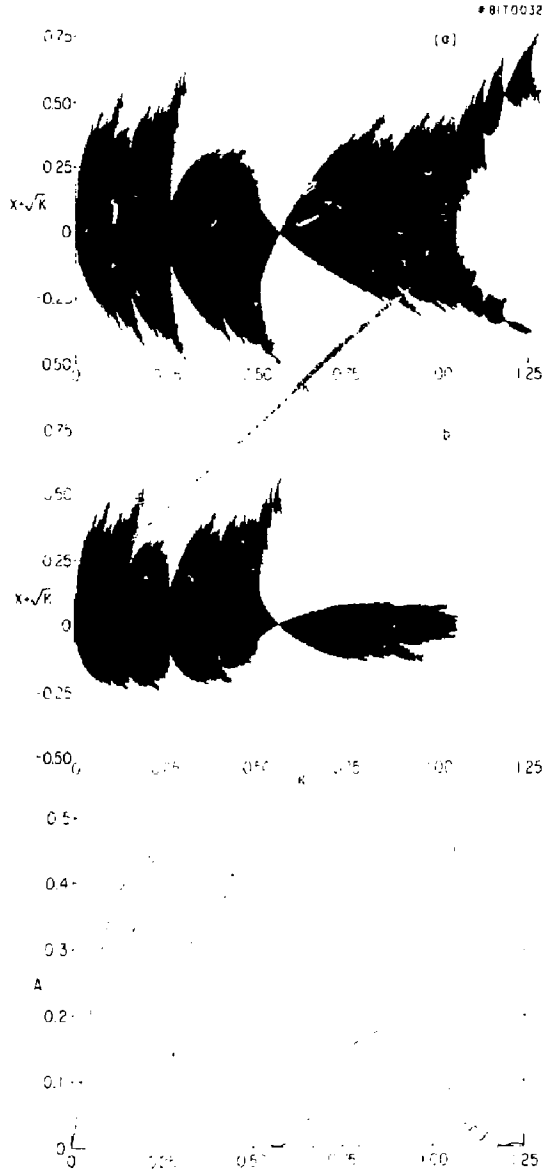
#81T0032
(a)
0.75
0.50
0.25
X·√K
0
-0.25
-0.50
0
0.25
0.50
0.75
1.00
1.25
K
(b)
0.5
0.4
0.3
A
0.2
0.1
0

Figure 4